Cell

# MDC1 Directly Binds Phosphorylated Histone H2AX to Regulate Cellular Responses to DNA Double-Strand Breaks

Manuel Stucki,[1,4,5] Julie A. Clapperton,[2,4] Duaa Mohammad,[3] Michael B. Yaffe,[3] Stephen J. Smerdon,[2,*] and Stephen P. Jackson[1,*]
[1] The Wellcome Trust/Cancer Research UK Gurdon Institute and Department of Zoology, Cambridge University, Tennis Court Road, Cambridge CB2 1QN, United Kingdom
[2] MRC National Institute for Medical Research, Division of Protein Structure, The Ridgeway, Mill Hill, London NW7 1AA, United Kingdom
[3] Center for Cancer Research, Massachusetts Institute of Technology, 77 Massachusetts Avenue, Cambridge, MA 02139, USA
[4] These authors contributed equally to this work.
[5] Present address: Institute of Veterinary Biochemistry and Molecular Biology, University of Zürich, Winterthurerstrasse 190, CH-8057 Zürich, Switzerland.
*Contact: ssmerdo@nimr.mrc.ac.uk (S.J.S.); s.jackson@gurdon.cam.ac.uk (S.P.J.)
DOI 10.1016/j.cell.2005.09.038

## SUMMARY

Histone variant H2AX phosphorylation in response to DNA damage is the major signal for recruitment of DNA-damage-response proteins to regions of damaged chromatin. Loss of H2AX causes radiosensitivity, genome instability, and DNA double-strand-break repair defects, yet the mechanisms underlying these phenotypes remain obscure. Here, we demonstrate that mammalian MDC1/NFBD1 directly binds to phospho-H2AX (γH2AX) by specifically interacting with the phosphoepitope at the γH2AX carboxyl terminus. Moreover, through a combination of biochemical, cell-biological, and X-ray crystallographic approaches, we reveal the molecular details of the MDC1/NFBD1-γH2AX complex. These data provide compelling evidence that the MDC1/NFBD1 BRCT repeat domain is the major mediator of γH2AX recognition following DNA damage. We further show that MDC1/NFBD1-γH2AX complex formation regulates H2AX phosphorylation and is required for normal radioresistance and efficient accumulation of DNA-damage-response proteins on damaged chromatin. Thus, binding of MDC1/NFBD1 to γH2AX plays a central role in the mammalian response to DNA damage.

## INTRODUCTION

DNA double-strand breaks (DSBs) are highly toxic lesions that, if unrepaired or repaired incorrectly, can cause cell death, mutations, and chromosomal translocations and can lead to cancer. Cells react to DSBs by rapidly deploying a host of proteins to the damaged-chromatin regions. Some of these factors engage in DNA repair, while others trigger a signaling pathway (called the DNA-damage checkpoint) that delays cell-cycle progression and coordinates repair processes; together, these events comprise the DNA damage response (DDR). Some DDR factors have intrinsic affinity for free DNA ends, while others, many of which contain *BR*CA1 *c*arboxy-*t*erminal (BRCT) domains, accumulate in large nuclear aggregates that appear as IR-induced nuclear foci (IRIF) by fluorescence microscopy. Increasing evidence suggests that IRIF are required for accurate and coordinated DSB repair in the context of chromatin.

A key regulator of IRIF formation in mammalian cells is the histone H2A variant H2AX, a component of the nucleosome core structure that comprises 10%–15% of total cellular H2A in higher organisms (Fernandez-Capetillo et al., 2004). H2AX is phosphorylated extensively on a conserved serine residue at its carboxyl terminus (C terminus) in chromatin regions bearing DSBs, and this is mediated by members of the phosphoinositide-3-kinase-related protein kinase (PIKK) family (Rogakou et al., 1999). Of these PIKKs, ataxia telangiectasia mutated (ATM) and DNA-dependent protein kinase catalytic subunit (DNA-PKcs) phosphorylate H2AX in response to DSBs in a partially redundant manner (Falck et al., 2005; Stiff et al., 2004). Cells isolated from H2AX-deficient mice exhibit radiation-induced chromosomal aberrations, indicating that H2AX is involved in the signaling and/or repair of DSBs (Bassing et al., 2002; Celeste et al., 2002). Indeed, H2AX modulates both homologous recombination (HR) and nonhomologous end joining (NHEJ) pathways of DSB repair, although it

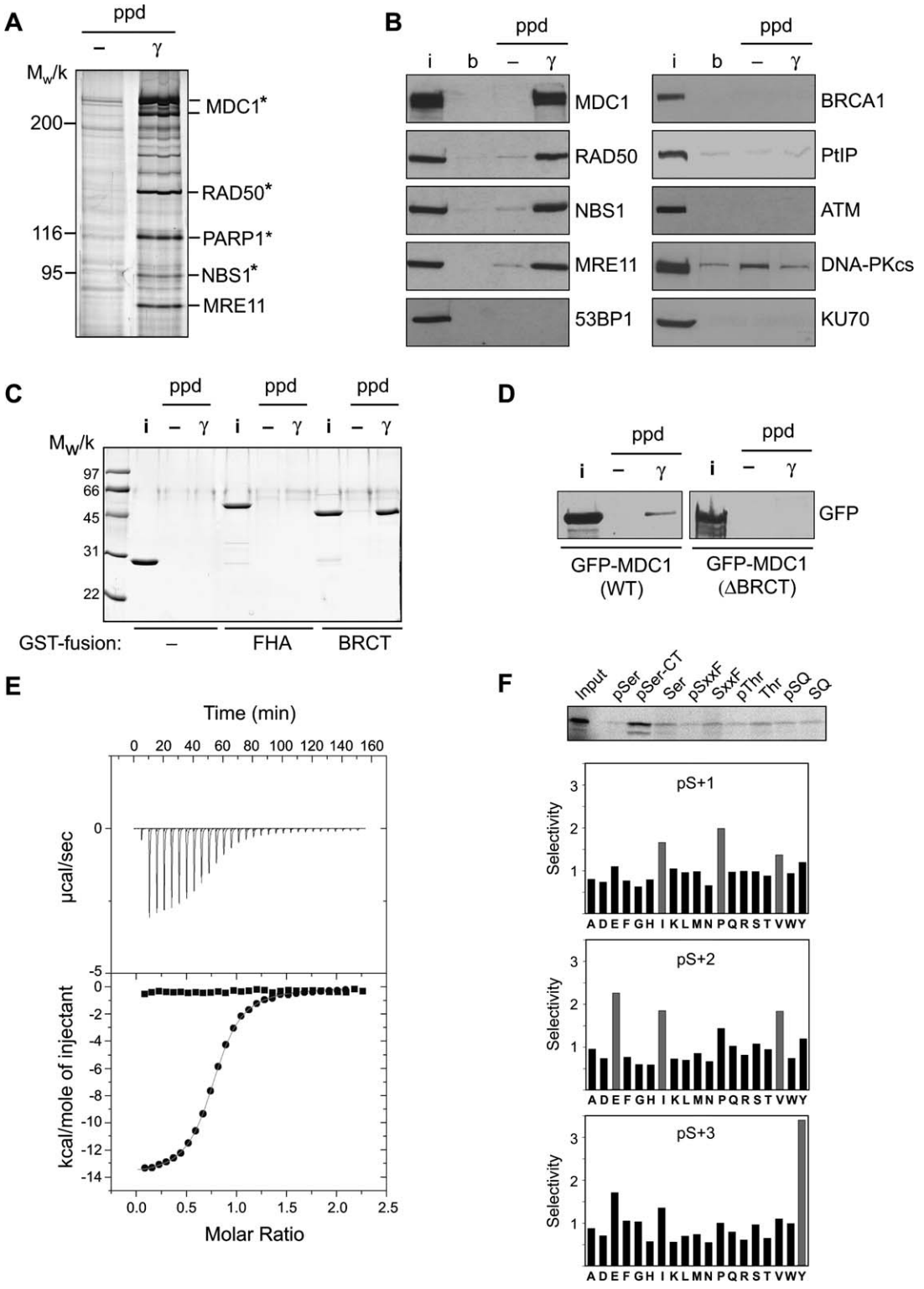


**Figure 1. MDC1 Interacts Directly with a H2AX Phosphopeptide via Its BRCT Domains**

(A) Silver-stained SDS-polyacrylamide gel of H2AX *p*eptide *p*ull-*d*own (ppd). "γ" represents the phosphopeptide; "–" represents its unphosphorylated derivative. Proteins marked by asterisks were identified by mass spectrometry.

(B) Western blot analysis of proteins pulled down by the H2AX phosphopeptide. "i" stands for input (10% of total protein input in the binding reaction); "b" stands for beads alone.

is not an essential component of either (Bassing et al., 2002; Celeste et al., 2002; Petersen et al., 2001; Xie et al., 2004). Interestingly, analysis of complemented *H2AX*$^{-/-}$ mouse cells showed that replacement of the phosphoacceptor serine residue at the H2AX C terminus with glutamic acid did not rescue the DSB hypersensitivity or IRIF defects of H2AX-deficient cells (Celeste et al., 2003a). This suggests that phosphorylation of the H2AX C-terminal tail creates an epigenetic signal that is recognized by one or more sensor proteins with specific affinity for the phosphoepitope. Here, we identify the tandem BRCT domain of MDC1/NFBD1 (henceforth named MDC1) as the predominant functional γH2AX phosphorecognition module in mammalian cells.

## RESULTS AND DISCUSSION

### MDC1 Interacts Directly with γH2AX via Its BRCT Domains

To identify proteins that bind the phosphorylated H2AX C terminus, we designed a phosphopeptide comprising the last 20 C-terminal residues of human H2AX phosphorylated on Ser139. The phosphopeptide and its unphosphorylated derivative were coupled to magnetic beads and used to retrieve (''pull down'') proteins from HeLa nuclear extracts. In contrast to the unphosphorylated peptide, the γH2AX phosphopeptide retrieved several proteins that appeared as predominant bands on an SDS-polyacrylamide gel (Figure 1A). Mass spectrometry revealed that the two prominent bands of ~250 kDa were MDC1 (the two bands likely represent splice variants), the bands of ~150 kDa and ~116 kDa were RAD50 and PARP1 respectively, and a somewhat weaker band of ~95 kDa was NBS1. While the presence of PARP1 in the pull-downs was not further analyzed, Western blot analyses with antibodies against human MDC1 and members of the MRE11/RAD50/NBS1 (MRN) complex confirmed the existence of these in the H2AX phosphopeptide pull-downs (Figure 1B). By contrast, 53BP1, BRCA1, and PTIP—BRCT-domain containing proteins that accumulate in IRIF and colocalize with γH2AX (Manke et al., 2003; Paull et al., 2000; Schultz et al., 2000)—were not efficiently retrieved by the γH2AX phosphopeptide. Furthermore, ATM, DNA-PKcs, and the NHEJ factor Ku70 also did not associate specifically with the γH2AX peptide. Weak association of ATM with the H2AX phosphopeptide was, however, detected in the absence of detergents in the washing buffer (data not shown). This is consistent with our earlier finding that ATM interacts directly with NBS1 (Falck et al., 2005) and that the interaction between ATM and NBS1 is weak in the absence of DNA and is disrupted by low detergent concentrations (Falck et al., 2005; You et al., 2005). Together with our previous finding that the association of the MRN complex with γH2AX depends on MDC1 (Lukas et al., 2004), these results indicate that MDC1 is the predominant γH2AX binding protein in nuclear extracts derived from cycling undamaged human cells.

**Table 1. ITC Binding Measurements of MDC1 and BRCA1 BRCT Domains with H2AX Peptides**

| Cell: BRCT Domain | Syringe: Peptide Sequence | $K_d$ (μM) |
|---|---|---|
| MDC1 BRCT WT | KKATQASQEY | NDB |
| | KKATQApSQEY | 2.2 |
| | KKApTQApSQEY | 2.0 |
| | KAPSGGKKATQApSQEY | 2.3 |
| | KKATQApSQEYAA | >500 |
| | KKATQApSQEA | NDB |
| | KKATQApSQEL | NDB |
| MDC1 BRCT K1936M | KKATQApSQEY | 90 |

NDB indicates no detectable heat change for MDC1 BRCT concentrations of at least 80 μM. pT and pS denote phosphothreonine and phosphoserine, respectively.

MDC1 contains two phosphospecific protein binding domains: an FHA domain at its N terminus and a tandem BRCT domain at its C terminus. However, phosphopeptide pull-down experiments with bacterially expressed GST fusions of these regions showed that only the tandem BRCT domain bound tightly and specifically to the γH2AX phosphopeptide (Figure 1C). Consistent with this, only wild-type MDC1 but not an MDC1 mutant lacking the BRCT domains (ΔBRCT) was retrieved from nuclear extracts of transfected 293T cells (Figure 1D). These results thereby establish that MDC1 interacts directly with the γH2AX phosphopeptide via its C-terminal BRCT domains.

By isothermal titration calorimetry (ITC) measurements, we established that the MDC1 BRCT region bound stoichiometrically to a 10 residue phosphopeptide corresponding to the γH2AX C terminus with an affinity of 2.2 μM (Figure 1E and Table 1), similar to previously characterized BRCT-phosphopeptide interactions (Manke et al., 2003; Rodriguez et al., 2003; Yu et al., 2003). The addition of 6 H2AX residues at

(C) Coomassie blue-stained SDS-polyacrylamide gel of an H2AX peptide pull-down experiment using purified GST-fusion fragments of the MDC1 FHA and BRCT domains.

(D) Western blot analysis of proteins pulled down by the H2AX peptides from nuclear extracts of full-length GFP-MDC1-transfected 293T cells. Blots were probed with an antibody against GFP.

(E) ITC binding isotherms show that the interaction between MDC1 BRCT and H2AX is phosphodependent. Symbols denote the following: ●, MDC1 BRCT binding to γ-H2AX phosphorylated on Ser139; ■, MDC1 BRCT titrated with nonphosphorylated H2AX peptide.

(F) Top: the MDC1 tandem BRCT domain binds to C-terminal phosphopeptide motifs. The peptide libraries used were pSer = XXXXpSXXXXXAKKK, pSer-CT = XXXXpSXXX, Ser = XXXXSXXXXXAKKK, pSF = XXXXpSXXFXXAKKK, SF = XXXXSXXFXXAKKK, pThr = XXXXpTXXXXXAKKK, Thr = XXXXTXXXXXAKKK, pSQ = XXXB(pS/pT)QJXXXAKKK, and SQ = XXXB(S/T)QJXXXAKKK. Bottom: the optimal motif of the tandem BRCTs of MDC1. Bar graphs show the relative abundance of each amino acid at a given cycle of sequencing compared to its abundance in the starting peptide library mixture.

the peptide's N terminus did not enhance binding (Table 1), so all further experiments were performed with derivatives of the shorter peptide. Although examination of the H2AX family reveals a second potential PIKK phosphorylation site in mammalian species (Redon et al., 2002), the doubly phosphorylated peptide bound MDC1 equivalently to the peptide phosphorylated on Ser139 alone (Table 1). Thus, if Thr136 is phosphorylated in vivo, it is unlikely to significantly affect γH2AX recognition by MDC1. Further analyses revealed that the residue at the pSer +3 position of γH2AX (Tyr142) is critical for MDC1 binding, as its substitution by Ala or Leu completely abrogated detectable binding to the MDC1 BRCT region (Table 1). Furthermore, the addition of 2 extra Ala residues to the C terminus of the γH2AX peptide dramatically weakened binding ($K_d$ > 500μM), indicating that the MDC1 BRCT region is unable to accommodate extra C-terminal residues.

## MDC1 Selects a γH2AX-like Motif in Oriented Library Screens

Oriented peptide library screening was used to define an optimal phosphopeptide binding motif for the MDC1 BRCT domain (Yaffe and Cantley, 2000). All libraries used in our initial experiments failed to bind the MDC1 tandem BRCT region in sufficient quantities for further analysis. These libraries all contained residues C-terminal to the +3 position, so on the basis of the dramatic loss of binding of C-terminally extended γH2AX phosphopeptides described above, we synthesized a new library extending only to the +3 position. This bound MDC1 BRCT in a phosphodependent manner with clear sequence selection in the more C-terminal residues (Figure 1F). The resulting motif, S-*P*/I/V-*E*/I/V-*Y*-*COOH*, is remarkably similar to the H2AX C-terminal sequence (SQEY-*COOH*). A related motif for the MDC1 BRCT region has been previously obtained from a C-terminally extended library (Rodriguez et al., 2003), but with additional selection of Phe at the +3 position. Thus, it would appear that the presence of the correct C terminus not only enhances overall binding but also confers a more pronounced Tyr +3 selectivity.

## Structure of the MDC1 BRCT-γH2AX Complex

To investigate the molecular basis for MDC1-γH2AX binding, we crystallized the MDC1 tandem BRCT domain with a dual-phosphorylated H2AX tail (KKA-pT136-QA-pS139-QEY; although pThr136 is superfluous for MDC1 binding, crystals grew more readily with this version of the peptide). The structure was determined by a single-wavelength anomalous dispersion experiment using selenomethionine-substituted MDC1 BRCT and refined at 2.4 Å, resulting in a crystallographic residual of 19.0% ($R_{free}$ 24.9%) and good stereochemistry (see Figure S1 in the Supplemental Data available with this article online for a segment of the final electron density map and Table S1 for crystallographic statistics). The final model comprises the conserved tandem BRCT domain of MDC1 (residues 1891–2082) and residues 138–142 of γH2AX for each of the two molecules in the asymmetric unit. Residues N-terminal to Ser139 are disordered in the structure, consistent with the absence of significant selection at these positions in the oriented library screens.

The 207 residue C-terminal fragment of MDC1 retains the typical tandem BRCT fold (Derbyshire et al., 2002; Joo et al., 2002; Williams et al., 2001) in which each BRCT repeat (BRCT 1 and BRCT 2) adopts a compact α/β fold and is connected by a linker region to form an extended structure ~70 Å long and ~35 Å in diameter (Figure 2A). The MDC1 BRCT region shows a conserved and characteristic assembly of the two tandem motifs mediated through extensive interactions between α2 of BRCT 1 and the α1′-α3′ pair of BRCT 2 with the BRCT-linker region. In MDC1, the 26 residue linker adopts a helix-loop-helix structure (αL1 and αL2) and makes contacts with both BRCT 1 and BRCT 2 at the domain interface. αL2 packs against the C terminus of the α2-α1′-α3′ triple-helix bundle, primarily via hydrophobic interactions with α2 and α3′, while αL1, which is unique to MDC1, has only limited contacts with the interface. γH2AX binds in an extended conformation to a groove at the interface between the two BRCT repeats, interacting with the β1/α1 loop and the N-terminal ends of α2 and α1′ (Figure 2A). Structure and sequence analysis of the MDC1 family reveals that the γH2AX binding groove has been highly conserved throughout evolution (Figure S2). Overall, the structure of the MDC1 BRCT-γH2AX complex explains the requirement for phosphorylation of H2AX Ser139, the overall sequence specificity, and the importance of a free C terminus apparent from our biochemical data (Figure 2B; see also below).

## A Conserved Phosphobinding Mode in MDC1 and BRCA1

Recent crystallographic and NMR studies have shown how the tandem BRCT domain from BRCA1 binds to phosphopeptides derived from BACH1 (Botuyan et al., 2004; Clapperton et al., 2004; Shiozaki et al., 2004) and a library screen (Williams et al., 2004). Superposition of the MDC1 BRCT-γH2AX structure with our BRCA1-BACH1 structure (Clapperton et al., 2004) results in a rms deviation of 1.8 Å for 146 matched Cα atoms (Figure S3). The overall location of the phosphopeptide is similar in both complexes, and both proteins bind the phosphate moiety through direct interactions with side- and main-chain atoms of three structurally conserved residues: Lys1936, Thr1898, and Gly1899 in MDC1 and Lys1702, Ser1655, and Gly1656 in BRCA1 (Figures 2C and 2D). Consistent with this, mutation of Lys1936 to Met reduces the affinity of MDC1 for γH2AX to ~90 μM as determined by ITC (Table 1). Even though the tandem BRCT domains of MDC1 and BRCA1 exhibit only 17% sequence identity, the direct protein-phosphate interactions—and even interactions mediated through the solvent lattice—are essentially identical. This extraordinary stereochemical similarity in phosphate binding by two such highly diverged BRCT tandem domains shows that phosphodependent binding is an important and ancient activity of BRCT tandem proteins.

## Sequence Specificity of MDC1-γH2AX Binding

Our in vitro peptide library screens and ITC data show a marked selectivity for tyrosine at the +3 position. Tyr142

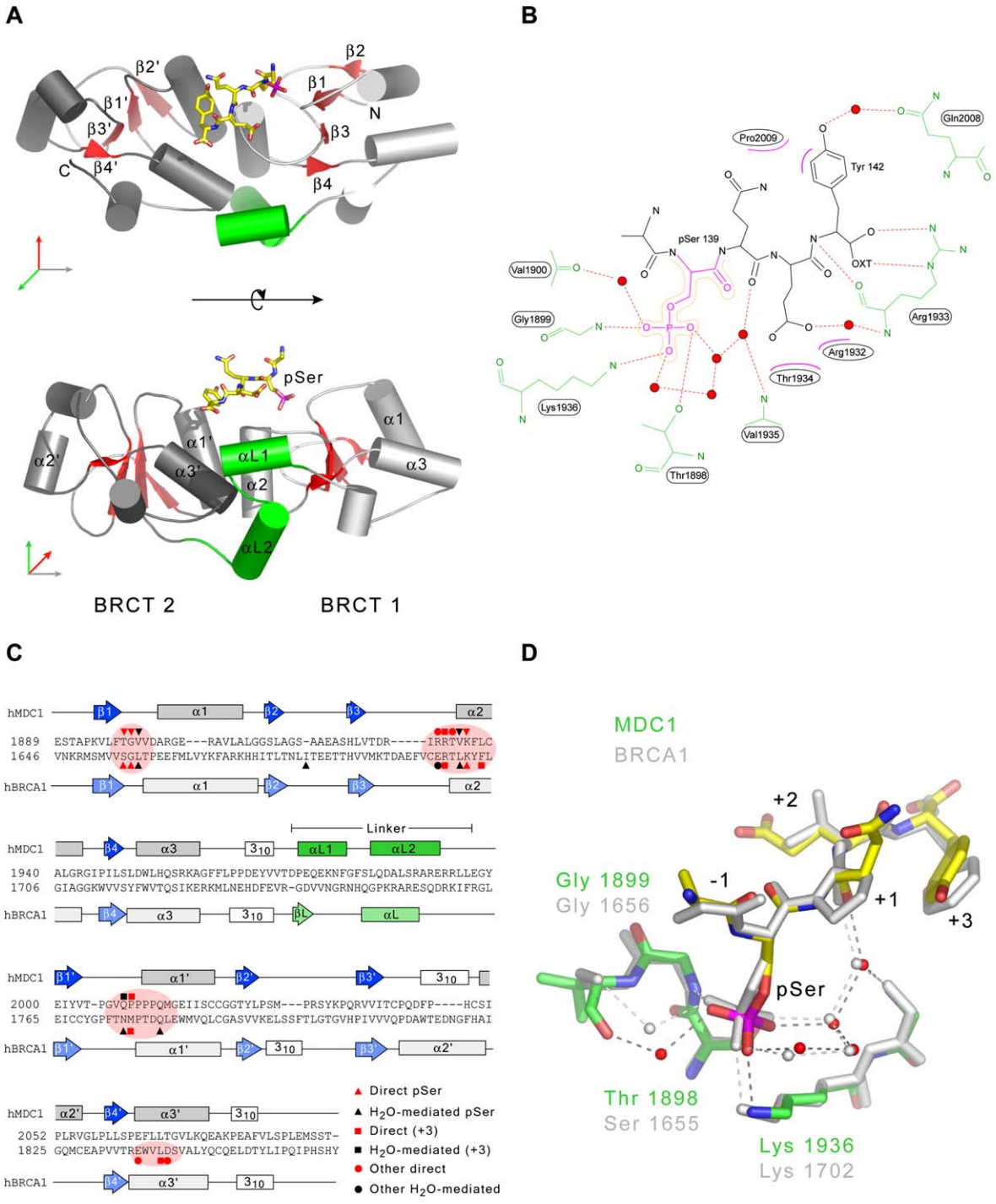


**Figure 2. Structure of the MDC1 BRCT-γ-H2AX Tail Complex**

(A) Ribbon representation of the MDC1 BRCT-γH2AX tail complex. The γH2AX peptide (yellow stick model) binds at the interface between the two BRCT repeats. The BRCT repeat linker is colored green.

(B) Schematic representation of protein-peptide contacts between MDC1 BRCT and the γH2AX tail. Hydrogen bonds, van der Waals interactions, and water molecules are denoted by dashed lines, pink crescents, and red circles, respectively.

(C) Structure-based sequence alignment of the tandem BRCT domains of MDC1 and BRCA1. Regions shaded with pink spheres highlight residues involved in phosphopeptide recognition.

(D) Detailed ball-and-stick superposition of the phosphate binding pockets from MDC1 BRCT-γH2AX and BRCA1 BRCT-BACH1 complexes. Water molecules are shown as red (MDC1) or white (BRCA1) spheres.

of γH2AX sits at the interface between the two BRCT repeats, with its phenolic side chain making favorable ring-stacking interactions with Pro2009 from a Pro-rich region in the β1′-α1′ loop that is characteristic of MDC1 orthologs (Figure 2B). Selection for Tyr rather than Phe is apparently explained by a water-mediated hydrogen-bonding interaction with the side-chain amide group of Gln2008. Of the remaining two H2AX residues involved in the MDC1 interaction, selection for Glu at the pSer +2 position is consistent with the presence of Glu or Asp at this position in known H2AX sequences (Glu141 in human H2AX). Glu141 forms a water-mediated contact with Arg1933 via its carboxylate group, van der Waals interactions with Arg1932 and Thr1934, and electrostatic interactions with the basic region around Arg1932 that likely favors acidic side chains at +2 (Figure 2B). By contrast, Gln140, which forms part of the consensus "SQ" motif for PIKK phosphorylation of H2AX, is the only site that deviates from the H2AX-like motif derived from oriented library screens. Weak selection for Pro +1 may point to a role for MDC1 binding to proline-directed kinase phosphorylation sites in other contexts, although the MDC1 tandem BRCT region binds only very weakly ($K_d \sim 100$ μM) to a phosphopeptide containing a known pSPTF cyclin-CDK motif (data not shown). Regardless, the X-ray structure shows that the Gln +1 side chain is directed away from the MDC1 surface toward bulk solvent. This indicates that the +1 position plays only a minor role in determining MDC1 binding specificity but is instead a crucial determinant of H2AX phosphorylation by PIKKs. Interestingly, a search of human sequences in the SwissProt/TrEMBL databases with a variant of the selected motif S/T-X-E/I/V-Y-*COOH* (where X is any amino acid) identified only 12 matches. Of these, only 2, H2AX itself (H2AX_HUMAN) and a galactosyltransferase (B3G8_HUMAN) contain Gln +1, and none contain Pro/Ile/Val at this position. Thus, the MDC1 BRCT binding site is tailored to recognize a highly conserved, PIKK-phosphorylated C-terminal sequence motif that is rare or even unique in the human proteome.

## MDC1 Recognition of the γH2AX C Terminus

The importance of MDC1 specificity to the free pSer +3 C terminus characteristic of all known H2AX sequences is underlined by the adverse effect on binding of C-terminal extensions to the γH2AX phosphopeptide. Our X-ray structure shows that the C-terminal residue, Tyr142, sits above the patch of positive charge generated by MDC1 Arg1933 in the binding cleft (Figure 2D). Main-chain interactions between Arg1933 and the peptide are similar to those observed for Arg1699 in previous BRCA1 BRCT phosphopeptide structures. Indeed, the predicted structural homology of these residues has led to the suggestion of a potential role for MDC1 Arg1933 in binding to the H2AX C terminus (Glover et al., 2004). Our structure now shows that Arg1933 is indeed crucial to C-terminal recognition, but its interactions with the peptide differ from those made by Arg1699 of BRCA1 in two significant ways (Figure 3). First, Arg1933 sits higher in the binding cleft due to an altered hydrogen-bonding pattern of its terminal amino groups with a conserved Glu (MDC1 2063/BRCA1 1836) located on α3′. In addition, the free carboxyl group of the phosphopeptide is rotated with respect to the main-chain amide of the Phe993-Gln994 peptide bond in the BRCA1-BACH1 complex. As a result, Arg1933 of MDC1 is able to form a strong, dual salt-bridging interaction with the negatively charged carboxyl terminus, compared to the single, uncharged hydrogen bond formed by BRCA1 Arg1699 with the BACH1 main-chain carbonyl group. Thus, loss of affinity upon the addition of extra C-terminal residues is attributable to removal of one of the carboxylate oxygen atoms by peptide bond formation and associated loss of negative charge, along with resulting unfavorable changes in the orientation of the Tyr142 side chain with respect to the +3 binding surface.

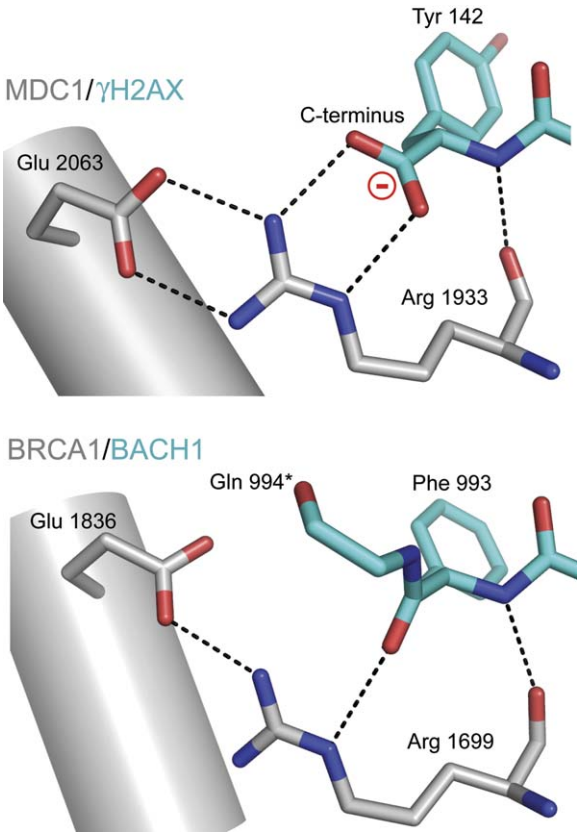


**Figure 3. MDC1 Recognition of the H2AX C Terminus**
Comparison of the structures of MDC1-γH2AX (top) and BRCA1-BACH1 (bottom) shows a rearranged hydrogen-bonding pattern involving the Arg1933 side chain that optimally presents it to the charged H2AX C terminus. *The side-chain atoms of Gln994 have been removed for clarity.

## Conserved Residues within the MDC1 BRCT Region and at the H2AX C Terminus Are Essential for Stable MDC1-γH2AX Association and MDC1 IRIF Formation In Vivo

Analysis of the MDC1 BRCT-γH2AX cocrystal structure revealed that 3 residues of BRCT 1 engage in direct hydrogen-bond interactions with γH2AX: Thr1898 and Lys1936

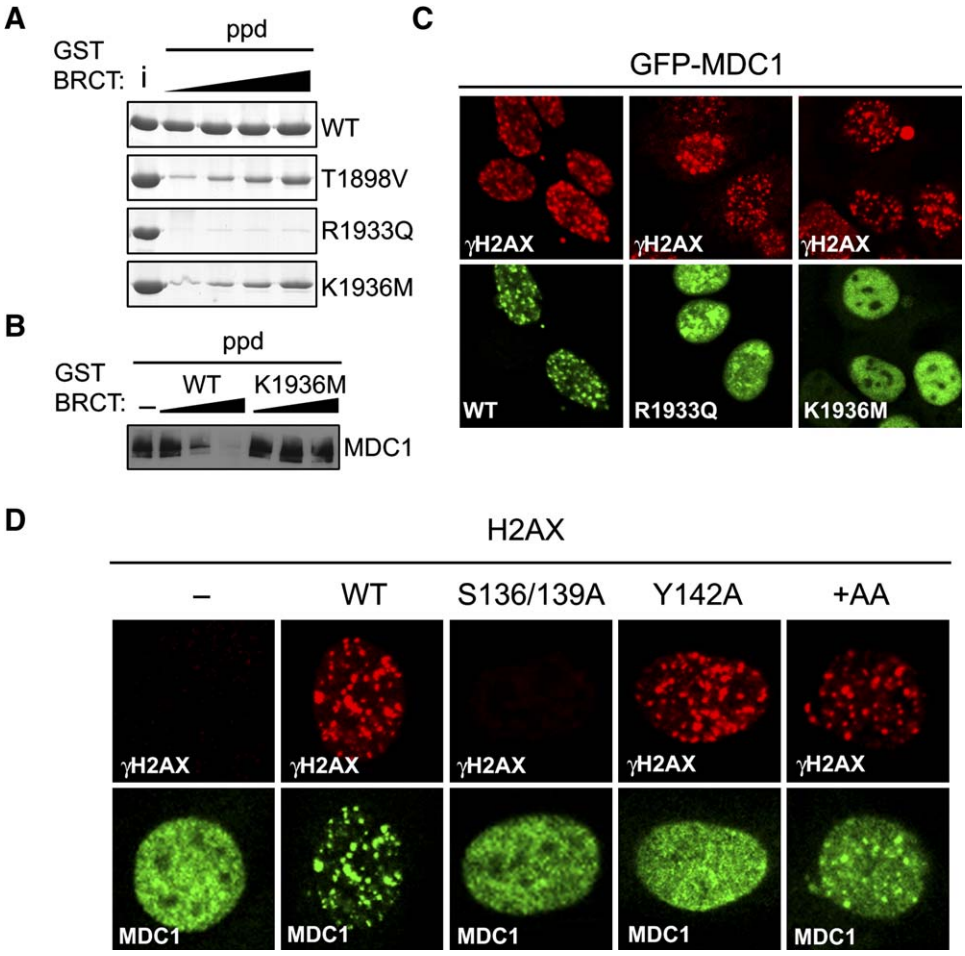


**Figure 4. Conserved Residues within the Tandem BRCT Domain and at the H2AX C Terminus Are Essential for Stable MDC1-γH2AX Association and MDC1 IRIF Formation**

(A) Phosphopeptide pull-down titration analysis of wild-type and mutant purified GST-BRCT fragments. The GST-BRCT concentrations were 2.5, 10, 50, and 250 μg/ml, respectively. The amount of protein loaded in the input lane (i) was 2.5 μg.

(B) Molecular competition experiment for phosphopeptide binding by endogenous MDC1 in HeLa nuclear extract and purified GST-BRCT fusion protein. GST-BRCT concentration was 2.5, 50, and 250 μg/ml, respectively.

(C) IRIF formation of recombinant wild-type and mutant GFP-MDC1 fusion proteins (full-length) 1 hr after 10 Gy of IR in transiently transfected 293T cells.

(D) IRIF formation of endogenous MDC1 1 hr after 10 Gy in *H2AX*$^{-/-}$ *p53*$^{-/-}$ MEFs stably transfected with wild-type or mutant mouse H2AX.

contact the phosphoserine, and Arg1933 contacts both the peptide backbone and the C-terminal carboxylate group. Significantly, mutation of Arg1933 to Gln (R1933Q) completely abolished detectable phosphopeptide binding by the MDC1 BRCT region, while mutating the two phosphoserine-contacting residues had a less dramatic impact but still significantly decreased binding (Figure 4A). The partial defects of the T1898V and K1936M mutants can be explained by a synergistic contribution of both phosphoserine-contacting residues to the overall stability of the complex. However, unlike the situation for the intact BRCT domain, the weak residual phosphopeptide binding activity of the K1936M mutant was insufficient for it to competitively inhibit binding of full-length HeLa cell MDC1 to the γH2AX phosphopeptide (Figure 4B). Consistent with the MDC1-γH2AX interaction being important for MDC1 IRIF formation, we found through transient transfection studies that, while full-length MDC1 fused to GFP formed IRIF effectively, the R1933Q and K1936M point-mutated derivatives did not (Figure 4C).

Next, we determined the effect of mutating the H2AX C terminus on MDC1 IRIF formation. Consistent with previous reports, we found that *H2AX*$^{-/-}$ *p53*$^{-/-}$ mouse embryonic fibroblasts (MEFs) were defective for MDC1 IRIF formation (Figure 4D; Lee et al., 2005; Stewart et al., 2003). However, while reintroducing a genomic fragment carrying the entire H2AX transcriptional unit (Celeste et al., 2003b) rescued the MDC1 IRIF defect of *H2AX*$^{-/-}$ *p53*$^{-/-}$ MEFs, expression of a H2AX mutant in which the two phosphoacceptor Ser residues were changed to Ala (S136/139A) did not. Interestingly, reintroducing into *H2AX*$^{-/-}$ *p53*$^{-/-}$ MEFs H2AX mutants in which the very C terminus was altered resulted in cell

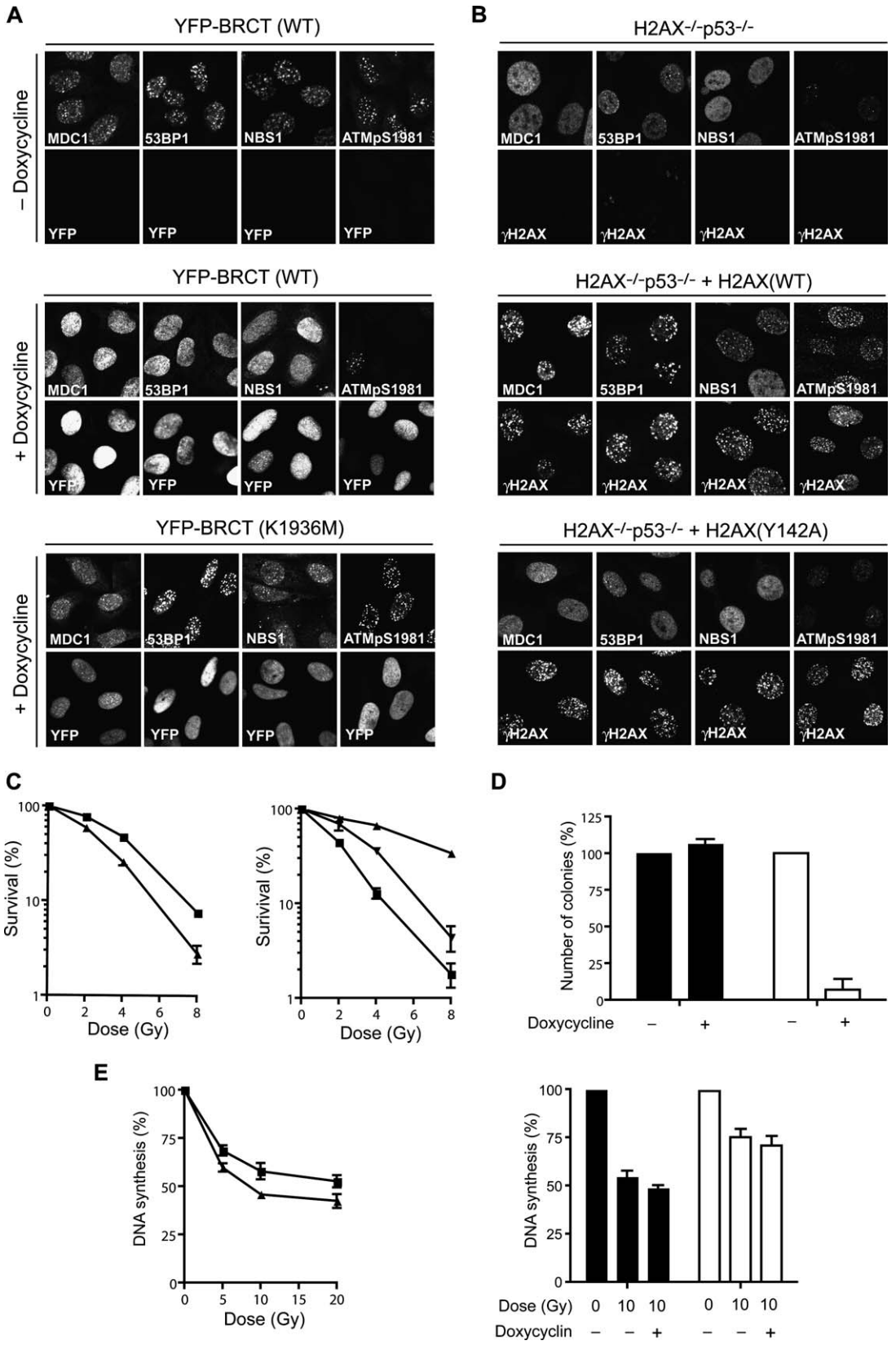
A
YFP-BRCT (WT)
– Doxycycline
MDC1
53BP1
NBS1
ATMpS1981
YFP
YFP-BRCT (WT)
+ Doxycycline
YFP-BRCT (K1936M)
+ Doxycycline
B
H2AX-/-p53-/-
γH2AX
H2AX-/-p53-/- + H2AX(WT)
H2AX-/-p53-/- + H2AX(Y142A)
C
Survival (%)
Dose (Gy)
Surivival (%)
D
Number of colonies (%)
Doxycycline
E
DNA synthesis (%)
Dose (Gy)
Doxycyclin

lines with seemingly normal H2AX phosphorylation and γH2AX IRIF formation but with severe defects in MDC1 accumulation. Thus, changing the C-terminal Tyr to Ala (Y142A) led to a complete defect in MDC1 IRIF formation, while extension of the H2AX C-terminal tail by two Ala residues (+AA) significantly reduced the size and intensity of MDC1 IRIF and increased pan-nuclear MDC1 staining (Figure 4D). Together, these data show that mutating MDC1 or H2AX in ways that impair the MDC1-γH2AX interaction leads to defects in MDC1 IRIF formation.

### Interaction between MDC1 and γH2AX Is Required for Efficient Accumulation of 53BP1, NBS1, and Phosphorylated ATM at Sites of Damaged Chromatin

To establish whether the MDC1-γH2AX interaction recruits other DDR factors to regions of damaged chromatin, we created U2OS cell lines carrying stably integrated, tetracycline-regulated expression cassettes directing the expression of wild-type or K1936M mutant MDC1 tandem BRCT derivatives fused to yellow fluorescent protein (YFP). As shown in Figure 5A, and consistent with previous reports (Shang et al., 2003; Xu and Stern, 2003), overexpression of the wild-type MDC1 BRCT region prevented IRIF formation by MDC1, 53BP1, NBS1, and Ser1981-phosphorylated ATM (ATM activation involves its autophosphorylation on Ser1981, and this autophosphorylated species forms IRIF; Bakkenist and Kastan, 2003). By contrast, when the K1936M mutant was overexpressed, MDC1, 53BP1, NBS1, and phospho-S1981 ATM formed IRIF in a manner indistinguishable from that in cells not expressing the YFP-BRCT construct (i.e., in noninduced cells; Figure 5A, compare top and bottom panels). Overexpression of the R1933Q mutant also did not affect MDC1, 53BP1, NBS1, and phospho-S1981 ATM IRIF formation (data not shown). Thus, the binding of the isolated MDC1 BRCT region to γH2AX prevents IRIF formation by endogenous MDC1 and also blocks the accumulation of other DDR factors at sites of DNA damage.

As a complementary approach to investigate the importance of the MDC1-γH2AX interaction, we exploited our finding that *H2AX*$^{-/-}$ *p53*$^{-/-}$ MEFs stably expressing the H2AX Y142A mutant displayed H2AX phosphorylation and γH2AX IRIF formation but not MDC1 IRIF formation (Figure 4D). Consistent with previous reports (Celeste et al., 2002; Stewart et al., 2003; Ward et al., 2003), we found that MDC1, 53BP1, and NBS1 did not form detectable IRIF in *H2AX*$^{-/-}$ *p53*$^{-/-}$ MEFs (Figure 5B, top panel), whereas they formed normally in *H2AX*$^{-/-}$ *p53*$^{-/-}$ MEFs complemented with wild-type H2AX (Figure 5B, middle panel). Similarly, the Ser1981-autophosphorylated ATM formed foci in an H2AX-dependent fashion (Figure 5B). Strikingly, while γH2AX foci were detected by antibodies in *H2AX*$^{-/-}$ *p53*$^{-/-}$ MEFs complemented with the Y142A mutant, no IRIF for MDC1, 53BP1, or NBS1 were observed in such cells (Figure 5B, bottom panel). Furthermore, while ATM autophosphorylation still occurred in *H2AX*$^{-/-}$ *p53*$^{-/-}$ MEFs and in *H2AX*$^{-/-}$ *p53*$^{-/-}$ MEFs complemented with the Y142A mutant of H2AX (data not shown), phosphorylated ATM did not form foci in such cells; instead, weak pan-nuclear staining of phospho-Ser1981 ATM was observed (Figure 5B, bottom panel). Thus, mutation of H2AX to a form that can still be phosphorylated but no longer binds MDC1 abrogates IRIF formation by all DDR factors studied.

The above results establish the MDC1-γH2AX interaction as a critical determinant for IRIF formation. This is perhaps most simply explained for the MRN complex, which interacts directly with MDC1 (Goldberg et al., 2003). Furthermore, as foci formation by phosphorylated ATM requires interactions between it and the NBS1 C terminus (Falck et al., 2005), an inability to form MRN IRIF presumably causes defective phospho-ATM foci in cells disrupted for the MDC1-γH2AX interaction. For 53BP1, however, the situation is likely to be more complex as its binding to chromatin at DSB sites is thought to be directed by histone methylation (Huyen et al., 2004). On the other hand, efficient 53BP1 accumulation at sites of DSBs also requires γH2AX (Celeste et al., 2002; Ward et al., 2003) and a functional MDC1-γH2AX interaction (this study), indicating that binding to methylated histones is not sufficient for 53BP1 IRIF formation. This interpretation is consistent with a recent report identifying MDC1 as a key upstream determinant of the dynamic assembly and

**Figure 5. Direct Interaction between MDC1 and γH2AX Is Required for 53BP1, NBS1, and Phospho-ATM IRIF Formation and for Normal Radioresistance but Not for Activation of the Intra-S Phase Checkpoint**

(A) MDC1, 53BP1, NBS1, and phospho-S1981 ATM IRIF analysis 30 min after 3 Gy in inducible U2OS YFP-BRCT-overexpressing cells. Noninduced cells (top), wild-type YFP-BRCT-expressing cells (middle), and K1936M YFP-BRCT-expressing cells (bottom).

(B) Analysis of MDC1, 53BP1, NBS1, and phospho-S1981 ATM IRIF formation 30 min after 3 Gy in *H2AX*$^{-/-}$ *p53*$^{-/-}$ MEFs (top) and *H2AX*$^{-/-}$ *p53*$^{-/-}$ MEFs stably complemented with wild-type (WT) mouse H2AX (clone WT4D; middle) and Y142A mutant H2AX (clone YA2A; bottom).

(C) Left graph: overexpression of the MDC1 BRCT domains radiosensitizes human cells. Expression of wild-type YFP-BRCT fusion protein was induced 8 hr before irradiation (triangles); mock-induced cells (squares) were used as negative control. Right graph: expression of wild-type mouse H2AX (triangles) rescues the radiosensitivity phenotype of *H2AX*$^{-/-}$ *p53*$^{-/-}$ MEFs (squares), but expression of Y142A mutated H2AX (inverted triangles) does not. Data are presented as mean ± standard deviation.

(D) Overexpression of the MDC1 BRCT domains yields a strong defect in random plasmid integration. Expression of wild-type YFP-BRCT fusion protein (empty bars) and K1936M mutant (filled bars) was induced 8 hr before transfection. Twenty-four hours later, cells were replated at low density in selective medium, and colonies were counted 10 days later. Data are presented as mean ± standard deviation.

(E) Left graph: overexpression of the MDC1 BRCT domains does not trigger an intra-S phase checkpoint defect. Expression of wild-type YFP-BRCT fusion protein was induced 8 hr before irradiation (triangles); mock-induced cells (squares) served as control. The rate of DNA synthesis was determined 1 hr after irradiation. Right graph: transient depletion of endogenous MDC1 by siRNA partially abrogates the intra-S phase checkpoint regardless of whether or not MDC1 is proficient for γH2AX binding. DNA synthesis was measured after transfection with MDC1-targeting siRNA (empty bars) and luciferase control siRNA (filled bars). Expression of the YFP-BRCT fusion protein was induced 8 hr before irradiation as indicated. Data are presented as mean ± standard deviation.

sustained retention of 53BP1 at DSB sites (Bekker-Jensen et al., 2005). Although it remains to be established whether MDC1 influences 53BP1 accumulation through regulation of γH2AX maintenance (Stewart et al., 2003) or by modulating chromatin in a way that permits efficient 53BP1 accumulation, the latter model is attractive because it may explain why low MDC1 expression is sufficient for seemingly normal 53BP1 accumulation at early time points after damage induction (Figure S4; Goldberg et al., 2003; Mochan et al., 2003; Peng and Chen, 2003) while deletion of H2AX or abrogation of the MDC1-γH2AX interaction prevents 53BP1 accumulation.

### The MDC1-γH2AX Interaction Is Needed for Normal Radioresistance but Not for Activation of the Intra-S Phase Checkpoint

To explore the physiological role (or roles) of the MDC1-γH2AX interaction, we used the systems developed above in which the interaction was abrogated by overexpression of the MDC1 BRCT region or by H2AX mutations. Significantly, colony-survival analyses after IR treatment revealed that overexpression of the MCD1 BRCT domains rendered human U2OS cells radiosensitive (Figure 5C, left graph), whereas overexpression of the K1936M mutant did not (data not shown; we chose the K1936M and not the R1933Q mutant as a negative control because it is structurally neutral, while Arg1933 plays an important structural role in BRCT tandem domains through interactions with the C-terminal helix α3′). Furthermore, while transfection with a vector expressing wild-type H2AX effectively rescued the radiosensitivity of *H2AX*$^{-/-}$ *p53*$^{-/-}$ MEFs (Figure 5C, right graph), expression of the H2AX Y142A mutant yielded an intermediate phenotype: much less resistant than cells expressing wild-type H2AX, but somewhat more resistant than noncomplemented *H2AX*$^{-/-}$ *p53*$^{-/-}$ MEFs. These results demonstrate that, while additional MDC1-independent functions for γH2AX cannot be excluded, a functional MDC1-γH2AX interaction is crucial for normal radioresistance in both p53-positive human U2OS cells and p53-deficient mouse cells.

As decreased radioresistance can indicate a defect in DSB repair, we tested whether disruption of the MDC1-γH2AX interaction interfered with DSB rejoining. While we did not detect a significant DSB repair defect in YFP-BRCT-overexpressing cells when we analyzed them by pulsed-field gel electrophoresis (data not shown), YFP-BRCT-overexpressing cells—but not cells overexpressing the K1936M mutant—had a dramatic defect in random plasmid integration (Figure 5D; YFP-BRCT overexpression did not reduce cell survival or plating efficiency in the absence of exogenous DNA damage, data not shown). These findings are consistent with a recent report showing that depletion of MDC1 by siRNA reduced random-plasmid-integration frequency in human cells (Lou et al., 2004) and indicate that, while not essential for NHEJ, the MDC1-γH2AX interaction is required for a subset of DNA end-joining events.

When damaged by IR during S phase, mammalian cells transiently reduce DNA synthesis in a manner partially dependent on MDC1 but independent of H2AX (Celeste et al., 2002; Goldberg et al., 2003; Lou et al., 2003; Stewart et al., 2003). This suggests that MDC1 influences the intra-S phase checkpoint through a mechanism that does not depend on its interaction with γH2AX. Indeed, cells overexpressing the YFP-BRCT fusion construct of MDC1 displayed even more efficient reduction of DNA synthesis after irradiation than noninduced control cells (Figure 5E, left graph). Furthermore, when the inducible U2OS cells were depleted of endogenous MDC1 by siRNA transfection, they displayed a partial defect in IR-induced reduction of DNA synthesis regardless of whether or not they overexpressed the YFP-BRCT construct (Figure 5E, right graph). These results confirm that regulation of the intra-S phase checkpoint by MDC1 is mechanistically distinct from its γH2AX binding function. In this context, it is interesting to note that overexpression of the MDC1 FHA domain triggers a pronounced intra-S phase checkpoint defect (Goldberg et al., 2003). The FHA domain of MDC1 does not bind to γH2AX (Figure 1C), but it interacts with the MRN complex (Goldberg et al., 2003). Thus, it is possible that MDC1 is composed of at least two functionally distinct regions, each carrying a phosphodependent protein interaction module: the N-terminal region that contains the FHA domain may control crosstalk between MDC1 and the MRN complex to mediate checkpoint activation, whereas the C-terminal BRCT region is required for sustained interactions with γH2AX to form IRIF that facilitate efficient DSB repair.

### MDC1 Controls H2AX Phosphorylation by Two Synergistic Mechanisms

Although it has been proposed that MDC1 is involved in the regulation of H2AX phosphorylation (Stewart et al., 2003), it is not known whether MDC1 controls initial H2AX phosphorylation, γH2AX maintenance, or both. To address this issue, we created a U2OS cell line containing a stably integrated MDC1-targeting small hairpin RNA (shRNA) expression cassette that silenced MDC1 expression with high efficiency (see Figure S4A); we then examined these and control cells for H2AX phosphorylation in response to IR (Figure 6A). Consistent with earlier findings (Rogakou et al., 1998), in control cells expressing a LacZ-targeting shRNA, H2AX phosphorylation levels reached a maximum ~10 min after IR treatment, started to decline between 1 and 2 hr, and reached background levels 8 to 12 hr postirradiation. Notably, in MDC1-depleted cells, the initial H2AX phosphorylation was similar to that in control cells, but it then declined much more rapidly than in control cells and had already reached background levels between 4 and 8 hr after damage induction. Thus, downregulation of MDC1 expression to low levels does not prevent γH2AX formation but instead impacts on γH2AX maintenance.

One explanation for the above observation is that MDC1 may protect γH2AX from premature dephosphorylation by physically preventing access to the phospho-Ser139 site by phosphatases. Consistent with this idea, a purified GST fusion containing the MDC1 tandem BRCT domain prevented λ-phosphatase from dephosphorylating a γH2AX phosphopeptide in vitro, whereas the K1936M mutant

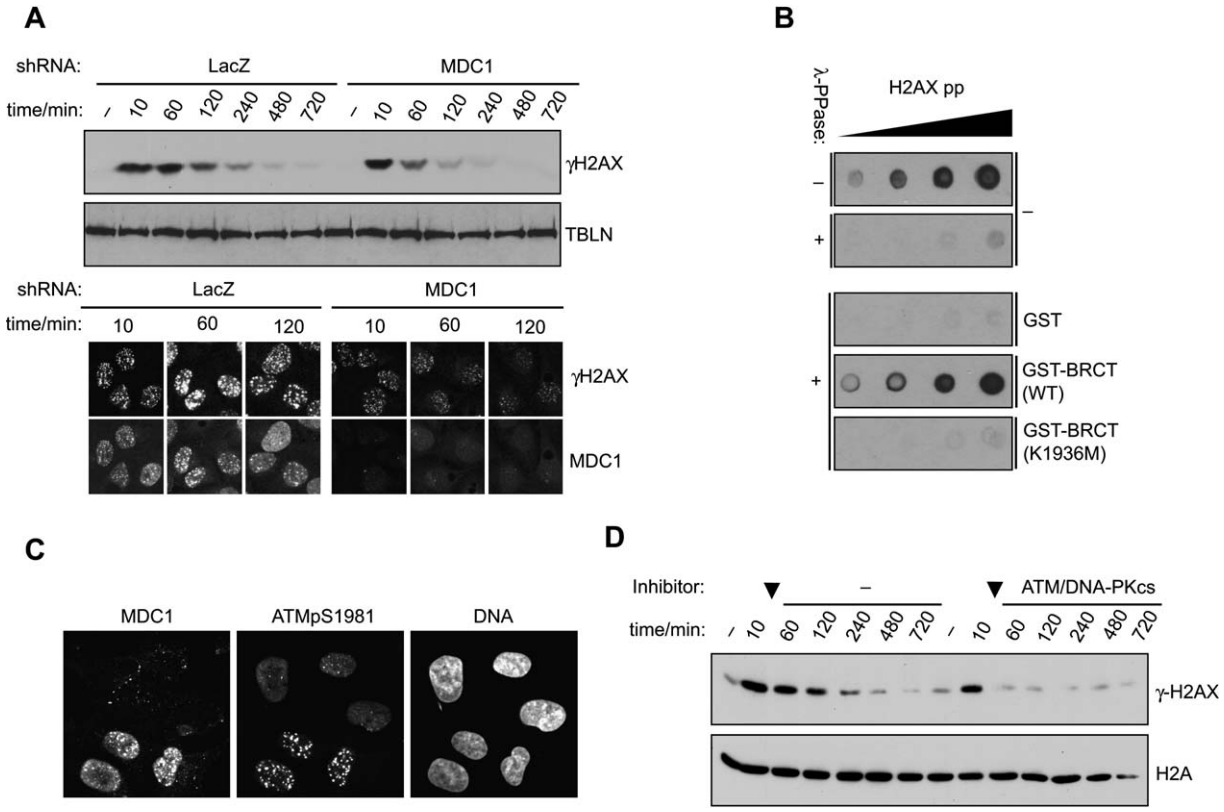


**Figure 6. MDC1 Controls γH2AX Maintenance by Two Synergistic Mechanisms**

(A) H2AX phosphorylation analysis of MDC1-depleted U2OS cells. Time-course analysis of H2AX phosphorylation by immunoblotting after 10 Gy of IR (upper); time-course analysis of γH2AX IRIF by immunofluorescence after 3 Gy of IR (lower).

(B) In vitro phosphatase protection assay. H2AX phosphopeptide was preincubated with GST and GST-BRCT fusion protein as indicated for 10 min at room temperature, followed by addition of λ-phosphatase and incubation at 30ºC for 30 min. SDS gel loading buffer was added, and the reaction was stopped by heating to 95ºC. Increasing amounts of reaction products were spotted on nitrocellulose, followed by phosphopeptide detection with a specific phospho-S139 H2AX antibody.

(C) MDC1-depleted cells were mixed with control cells and irradiated with 6 Gy of IR. One hour after treatment, cells were fixed and immunostained as indicated.

(D) H2AX phosphorylation time-course analysis in U2OS cells pretreated with 10 Gy of IR and in the presence or absence of ATM and DNA-PKcs inhibitors. Arrowheads indicate the time point of addition of inhibitor and mock-inhibitor solution, respectively (15 min after irradiation).

protein did not (Figure 6B). Also supporting a role for MDC1 in regulating γH2AX dephosphorylation, we found that U2OS cells expressing the MDC1 tandem BRCT domain-YFP fusion displayed higher levels of H2AX phosphorylation than control cells (Figure S5B). Furthermore, pan-nuclear background γH2AX staining was generally observed in YFP-BRCT-expressing cells, and the intensity of this staining correlated with the extent of YFP-BRCT overexpression (Figure S5C). Although the mechanism of γH2AX removal in mammalian cells is not yet understood and the phosphatase responsible for dephosphorylation of Ser139 has yet to be identified, these findings suggest that one mechanism by which MDC1 regulates γH2AX maintenance involves its control of γH2AX dephosphorylation.

It has recently been demonstrated that MDC1 undergoes a dynamic exchange between the chromatin flanking the sites of DSBs and the neighboring nucleoplasm, with the mean residence time at the damage sites of only 6.7 s (Lukas et al., 2004). Such a rapid exchange is likely to provoke repeated phosphorylation/dephosphorylation cycles of H2AX in damaged-chromatin regions. Thus, another way that MDC1 might influence γH2AX maintenance is by controlling ATM activity (Mochan et al., 2003). However, when we analyzed cells 1 hr after IR treatment, MDC1 depletion had no discernible effect on ATM Ser1981 phosphorylation or the phosphorylation state of several known ATM target proteins (CHK2, NBS1, SMC1, and p53), indicating that MDC1 depletion does not impair ATM activity per se (Figure S5A). Nevertheless, and consistent with data obtained in cells overexpressing the MDC1 BRCT region, MDC1 depletion led to consistent defects in IRIF formation by phospho-Ser1981 ATM (Figure 6C; this shows a mixed population of cells containing either a LacZ shRNA or an MDC1 shRNA, and ATM phospho-Ser1981 foci exist in the former but not the latter). These findings raised the possibility that MDC1 might influence H2AX phosphorylation by retaining active ATM

(and perhaps also DNA-PK) in damaged-chromatin regions. Since MDC1 is vital for the accumulation of active ATM on damaged chromatin, it is conceivable that the local concentration of active ATM at sites of damage mediated by MDC1 may shift the equilibrium of H2AX phosphorylation/dephosphorylation toward phosphorylation. For such a model to explain the premature loss of H2AX phosphorylation upon loss of the MDC1-γH2AX interaction, we reasoned that continual ATM and DNA-PK activity would be needed for maintaining normal H2AX phosphorylation. To test this, we treated cells with IR, incubated them for 10 min to allow H2AX phosphorylation, and then treated or mock treated them with small-molecule inhibitors of ATM and DNA-PKcs. While H2AX phosphorylation was maintained for several hours in the mock-treated cells, it was rapidly lost in the inhibitor-treated cells (Figure 6D; similar results were obtained with other PIKK targets such as CHK2 and SMC1; J. Falck, personal communication). This reveals that continued PIKK activity is required for normal γH2AX maintenance and suggests that MDC1-mediated PIKK accumulation promotes normal γH2AX maintenance. In addition, comparison of H2AX phosphorylation levels in wild-type and Y142A-complemented *H2AX*$^{-/-}$ *p53*$^{-/-}$ MEFs that expressed comparable amounts of total H2AX revealed significantly lower levels of H2AX phosphorylation in Y142A-complemented cells (Figure S5E). Based on these results, we suggest that MDC1 contributes to normal H2AX phosphorylation after IR both by protecting γH2AX from phosphatases and by promoting H2AX phosphorylation through its mediation of the retention of active ATM, and possibly also DNA-PK, in damaged-chromatin regions. It has so far not been possible to distinguish between the relative contributions of these mechanisms because disruption of the MDC1-γH2AX interaction or depletion of endogenous MDC1 interferes with both processes.

## Conclusions

We have presented biochemical, biological, and structural evidence indicating that MDC1 is the predominant γH2AX recognition module in higher eukaryotes. Firstly, we demonstrate that the BRCT tandem domain of MDC1 interacts tightly and specifically with a peptide representing the γH2AX C terminus and that binding is absolutely dependent on phosphorylation of Ser139, the ATM target site. Second, the X-ray structure of the MDC1-γH2AX complex reveals that the BRCT-domain binding cleft is exquisitely tailored to recognize the γH2AX motif and shows how the unusual—and possibly unique—proximity of the Ser139Gln140 PIKK phosphorylation site to the H2AX C terminus is detected. Finally, we show that the major function of this interaction is to promote accumulation and prolonged interaction of DDR factors in damaged-chromatin regions, a process that appears to be essential for efficient and accurate DSB repair but not for checkpoint activation. Together, our data demonstrate clear in vivo relevance of the direct interaction between MDC1 and γH2AX and have important mechanistic, biological, and evolutionary implications for our understanding of DNA-damage-initiated events in the context of chromatin.

## EXPERIMENTAL PROCEDURES

### Plasmids

MDC1 FHA-GST and MDC1 BRCT-GST were as described (Goldberg et al., 2003). Full-length wild-type and ΔBRCT GFP-MDC1 constructs were from P.-L. Chen (Shang et al., 2003). pSUPER-MDC1 and LacZ shRNA constructs have been described (Lukas et al., 2004). Full-length MDC1 and BRCT-only T1898V, R1933Q, and K1936M mutants were generated by the QuikChange Site-Directed Mutagenesis Kit (Stratagene). The YFP-BRCT construct comprised MDC1 residues 1883–2089 and a nuclear localization signal. To generate an inducible expression cassette, two tetracycline-repressor binding elements were inserted between promoter and coding sequences. The genomic fragment comprising the mouse H2AX coding and endogenous promoter sequences was a gift from A. Nussenzweig (Celeste et al., 2003b).

### Extract Preparation, Protein Expression, and Purification

Whole-cell extracts were prepared in SDS sample buffer or buffer A (50 mM Tris-HCl [pH 7.5], 200 mM NaCl, 0.5% NP-40, 1 mM dithiothreitol, 1 mM AEBSF). HeLa and 293T nuclear cell extracts were purchased from Computer Cell Culture Center (HeLa) or prepared according to Dignam et al. (1983). For H2AX peptide pull-downs, MDC1 BRCT domains were expressed as GST fusions in *E. coli* and purified on glutathione Sepharose (Amersham Pharmacia Biotech). For ITC and crystallization, proteins were synthesized in *E. coli* BL21 (Novagen) using the pGEX-4T1 vector (Amersham Pharmacia Biotech) by overnight shaking in LB at 18ºC and were purified by glutathione Sepharose affinity and S75 (Amersham Pharmacia Biotech) gel filtration chromatography following removal of glutathione S-transferase fusion with thrombin. MDC1 BRCT N-terminal limits were determined by Edman sequencing and electrospray mass spectrometry. Selenomethionine (SeMet) incorporated MDC1 BRCT was expressed in *E. coli* B834(DE3) cells (Novagen) and purified as for native protein.

### Peptide Binding

Synthetic peptides were from Dr. W. Mawby (University of Bristol). For pull-downs, biotinylated phosphopeptide (hH2AX 123–142) and its unphosphorylated derivative were coupled to streptavidin-coated Dynabeads M-280 (Dynal), incubated with HeLa or 293T nuclear extracts, and incubated with purified GST-BRCT fractions. Beads were washed extensively with Tris buffer saline (pH 7.5) containing 1% (v/v) Tween 20 and bound proteins subjected to SDS-PAGE and immunoblotting. Quantification of BRCT-phosphopeptide interaction was by ITC (Wiseman et al., 1989) with a MicroCal Omega VP-ITC calorimeter (MicroCal Inc., Northampton, MA). Proteins were dialyzed against ITC buffer (50 mM HEPES, 300 mM NaCl, 0.5 mM β-mercaptoethanol). Experiments were done at 20ºC and involved 30 successive 10 μl injections of 300–800 μM peptide solution into a sample cell containing 30–80 μM protein solution. Heats of dilution were subtracted and binding isotherms were plotted and analyzed with MicroCal Origin version 7.0, assuming a single-site binding model.

### Peptide Library Binding

Peptide library binding was done essentially as described (Yaffe and Cantley, 2000). For motif determination, a phosphoserine-oriented degenerate library of sequence KKKYAXXXXpSXXX (X denotes all amino acids except Cys) was synthesized. Screening was done with saturating amounts of GST-MDC1 BRCT (1–1.5 mg). Bound peptides were sequenced by automated Edman degradation on a Procise protein microsequencer. Selectivity values for each residue were determined by comparing the relative abundance (mole percentage) of each amino acid at a sequencing cycle in the recovered peptides to that of each amino acid in the original library mixture at the same position (Yaffe and Cantley, 2000).

### Crystallization and Structure Determination

Native and selenomethionine MDC1 BRCT (residues 1883–2089) were crystallized with a 1:2 stoichiometric excess of a doubly phosphorylated

H2AX peptide (KKA-pT136-QA-pS139-QEY) by hanging-drop vapor diffusion at 18ºC. Crystals grew from 1 μl protein-phosphopeptide complex (0.66 mM) and 1 μl reservoir solution (35%–37% PEG 4K, 0.4 M NaCl, and 0.1 M Tris-HCl [pH 8.5]) in space group $P2_12_12_1$ (a = 67.4 Å, b = 75.6 Å, c = 114.9 Å), with two molecules in the asymmetric unit. Crystals were dehydrated over a 50% w/v PEG 4K solution, equilibrated for 12 hr, and flash cooled directly from the mother liquor. Data from a single-wavelength anomalous dispersion experiment at the selenium edge were collected at the SRS Daresbury (Station 14.2) and processed using DENZO and SCALEPACK (Otwinowski and Minor, 1997). Four selenium-atom positions were located and refined using SOLVE, giving a figure of merit of 0.3 (Terwilliger and Berendzen, 1999). Phases were improved with RESOLVE (Terwilliger and Berendzen, 1999), resulting in a readily interpretable electron density map that was further improved by noncrystallographic symmetry averaging in DM (Cowtan and Main, 1996). Model building was carried out using O (Jones et al., 1991), and the structure was refined at 2.4 Å using REFMAC5 (Murshudov et al., 1997). Data-collection, phasing, and refinement statistics are summarized in Table S1 of the Supplementat Data. All structure figures were prepared with Pymol (http://pymol.sourceforge.net/).

### Cell Culture

Transfection of plasmids and siRNAs was with FuGene6 (Roche) or calcium phosphate and Oligofectamine (Invitrogen), respectively. Luciferase (CGUACGCGGAAUACUUCGAdTdT) and MDC1-targeting (GUCUCC CAGAAGACAGUGUdTdT) siRNA duplexes were from Dharmacon. Inhibitors of ATM (KU55933) (Hickson et al., 2004) and DNA-PKcs (NU7026) (Veuger et al., 2004) were used at 10 μM (gift from G. Smith). Complementation of *H2AX*$^{-/-}$ *p53*$^{-/-}$ MEFs was as described (Celeste et al., 2003b). Stable downregulation of MDC1 was as described (Lukas et al., 2004). Inducible YFP-BRCT-expressing cells were generated by transfection of a U2OS cell line expressing the tetracycline repressor (Invitrogen) with inducible YFP-BRCT expression plasmid encoding wild-type MDC1 BRCT domains or K1936M mutant followed by selection with neomycin (G418). Irradiation was done in a Faxitron X-ray cabinet at 3.15 Gy/min. Clonogenic survival and RDS assays were as described (Falck et al., 2005; Goldberg et al., 2003). Random plasmid integration was done by transfection of linearized pBabe-puro with LacZ expression plasmid. Twenty-four hours later, cells were replated at low density in puromycine-containing medium. and colonies were counted 10 days after transfection. A fraction of the transfected cells were stained with X-Gal to normalize for transfection efficiency.

### Antibodies and Immunofluorescence

Commercial antibodies used in this study were from Abcam (Chk2 and tubulin), Novus Biologicals (ATM and 53PB1), Upstate (γH2AX and H2A), Rockland Immunochemicals (pS1981-ATM), Bethyl Laboratories (H2AX, pS966-SMC1, and SMC1), Cell Signaling Technology (pS1981-ATM, pT68-Chk2, pS15-p53, pS343-Nbs1, and p53), Oncogene (Nbs1 and DNA-PKcs), BD Biosciences (YFP), Serotec (Ku70), and Santa Cruz Biotechnology (BRCA1). Monoclonal anti-GFP antibody was from Cancer Research UK. Rabbit and sheep antisera to MDC1, RAD50, NBS1, and MRE11 and rabbit antiserum for mouse MDC1 have been described (Goldberg et al., 2003; Lee et al., 2005). Purified sheep antibodies to human PTIP were from J. Rouse (Jowsey et al., 2004), and rabbit antiserum to mouse NBS1 was from A. Nussenzweig (Celeste et al., 2003b). For immunofluorescence staining, cells were grown on glass coverslips and fixed in ice-cold methanol or methanol/acetone.

### Supplemental Data

Supplemental Data include Supplemental References, one table, and five figures and can be found with this article online at http://www.cell.com/cgi/content/full/123/7/1213/DC1/.

## ACKNOWLEDGMENTS

We thank members of the Jackson and Smerdon laboratories for their suggestions; L. Haire for assistance with crystallization; J. Coates for help with tissue culture; and A. Nussenzweig, P.-L. Chen, J. Rouse, M. Goldberg, and G. Smith for reagents. We thank J. Falck, J. Downs, A. Nussenzweig, J. Lukas, and J. Chen for advice and for sharing unpublished results. This work was made possible through core funding by Cancer Research UK and the Wellcome Trust and was supported by Cancer Research UK and grant no. 823A-064719 from the Swiss National Foundation to M.S. S.J.S. is grateful for support from the Medical Research Council, UK.

Received: June 27, 2005
Revised: August 20, 2005
Accepted: September 19, 2005
Published: December 28, 2005

## REFERENCES

Bakkenist, C.J., and Kastan, M.B. (2003). DNA damage activates ATM through intermolecular autophosphorylation and dimer dissociation. Nature *421*, 499–506.

Bassing, C.H., Chua, K.F., Sekiguchi, J., Suh, H., Whitlow, S.R., Fleming, J.C., Monroe, B.C., Ciccone, D.N., Yan, C., Vlasakova, K., et al. (2002). Increased ionizing radiation sensitivity and genomic instability in the absence of histone H2AX. Proc. Natl. Acad. Sci. USA *99*, 8173–8178.

Bekker-Jensen, S., Lukas, C., Melander, F., Bartek, J., and Lukas, J. (2005). Dynamic assembly and sustained retention of 53BP1 at the sites of DNA damage are controlled by Mdc1/NFBD1. J. Cell Biol. *170*, 201–211.

Botuyan, M.V., Nomine, Y., Yu, X., Juranic, N., Macura, S., Chen, J., and Mer, G. (2004). Structural basis of BACH1 phosphopeptide recognition by BRCA1 tandem BRCT domains. Structure (Camb.) *12*, 1137–1146.

Celeste, A., Petersen, S., Romanienko, P.J., Fernandez-Capetillo, O., Chen, H.T., Sedelnikova, O.A., Reina-San-Martin, B., Coppola, V., Meffre, E., Difilippantonio, M.J., et al. (2002). Genomic instability in mice lacking histone H2AX. Science *296*, 922–927.

Celeste, A., Difilippantonio, S., Difilippantonio, M.J., Fernandez-Capetillo, O., Pilch, D.R., Sedelnikova, O.A., Eckhaus, M., Ried, T., Bonner, W.M., and Nussenzweig, A. (2003a). H2AX haploinsufficiency modifies genomic stability and tumor susceptibility. Cell *114*, 371–383.

Celeste, A., Fernandez-Capetillo, O., Kruhlak, M.J., Pilch, D.R., Staudt, D.W., Lee, A., Bonner, R.F., Bonner, W.M., and Nussenzweig, A. (2003b). Histone H2AX phosphorylation is dispensable for the initial recognition of DNA breaks. Nat. Cell Biol. *5*, 675–679.

Clapperton, J.A., Manke, I.A., Lowery, D.M., Ho, T., Haire, L.F., Yaffe, M.B., and Smerdon, S.J. (2004). Structure and mechanism of BRCA1 BRCT domain recognition of phosphorylated BACH1 with implications for cancer. Nat. Struct. Mol. Biol. *11*, 512–518.

Cowtan, K.D., and Main, P. (1996). Phase combination and cross validation in iterated density-modification calculations. Acta Crystallogr. D Biol. Crystallogr. *52*, 43–48.

Derbyshire, D.J., Basu, B.P., Serpell, L.C., Joo, W.S., Date, T., Iwabuchi, K., and Doherty, A.J. (2002). Crystal structure of human 53BP1 BRCT domains bound to p53 tumour suppressor. EMBO J. *21*, 3863–3872.

Dignam, J.D., Lebovitz, R.M., and Roeder, R.G. (1983). Accurate transcription initiation by RNA polymerase II in a soluble extract from isolated mammalian nuclei. Nucleic Acids Res. *11*, 1475–1489.

Falck, J., Coates, J., and Jackson, S.P. (2005). Conserved modes of recruitment of ATM, ATR and DNA-PKcs to sites of DNA damage. Nature *434*, 605–611.

Fernandez-Capetillo, O., Lee, A., Nussenzweig, M., and Nussenzweig, A. (2004). H2AX: the histone guardian of the genome. DNA Repair (Amst.) *3*, 959–967.

Glover, J.N., Williams, R.S., and Lee, M.S. (2004). Interactions between BRCT repeats and phosphoproteins: tangled up in two. Trends Biochem. Sci. *29*, 579–585.

Goldberg, M., Stucki, M., Falck, J., D'Amours, D., Rahman, D., Pappin, D., Bartek, J., and Jackson, S.P. (2003). MDC1 is required for the intra-S-phase DNA damage checkpoint. Nature *421*, 952–956.

Hickson, I., Zhao, Y., Richardson, C.J., Green, S.J., Martin, N.M., Orr, A.I., Reaper, P.M., Jackson, S.P., Curtin, N.J., and Smith, G.C. (2004). Identification and characterization of a novel and specific inhibitor of the ataxia-telangiectasia mutated kinase ATM. Cancer Res. *64*, 9152–9159.

Huyen, Y., Zgheib, O., Ditullio, R.A., Jr., Gorgoulis, V.G., Zacharatos, P., Petty, T.J., Sheston, E.A., Mellert, H.S., Stavridi, E.S., and Halazonetis, T.D. (2004). Methylated lysine 79 of histone H3 targets 53BP1 to DNA double-strand breaks. Nature *432*, 406–411.

Jones, T.A., Zou, J.Y., Cowan, S.W., and Kjeldgaard (1991). Improved methods for building protein models in electron density maps and the location of errors in these models. Acta Crystallogr. A *47*, 110–119.

Joo, W.S., Jeffrey, P.D., Cantor, S.B., Finnin, M.S., Livingston, D.M., and Pavletich, N.P. (2002). Structure of the 53BP1 BRCT region bound to p53 and its comparison to the Brca1 BRCT structure. Genes Dev. *16*, 583–593.

Jowsey, P.A., Doherty, A.J., and Rouse, J. (2004). Human PTIP facilitates ATM-mediated activation of p53 and promotes cellular resistance to ionizing radiation. J. Biol. Chem. *279*, 55562–55569.

Lee, A.C., Fernandez-Capetillo, O., Pisupati, V., Jackson, S.P., and Nussenzweig, A. (2005). Specific association of mouse MDC1/NFBD1 with NBS1 at sites of DNA-damage. Cell Cycle *4*, 177–182.

Lou, Z., Minter-Dykhouse, K., Wu, X., and Chen, J. (2003). MDC1 is coupled to activated CHK2 in mammalian DNA damage response pathways. Nature *421*, 957–961.

Lou, Z., Chen, B.P., Asaithamby, A., Minter-Dykhouse, K., Chen, D.J., and Chen, J. (2004). MDC1 regulates DNA-PK autophosphorylation in response to DNA damage. J. Biol. Chem. *279*, 46359–46362.

Lukas, C., Melander, F., Stucki, M., Falck, J., Bekker-Jensen, S., Goldberg, M., Lerenthal, Y., Jackson, S.P., Bartek, J., and Lukas, J. (2004). Mdc1 couples DNA double-strand break recognition by Nbs1 with its H2AX-dependent chromatin retention. EMBO J. *23*, 2674–2683.

Manke, I.A., Lowery, D.M., Nguyen, A., and Yaffe, M.B. (2003). BRCT repeats as phosphopeptide-binding modules involved in protein targeting. Science *302*, 636–639.

Mochan, T.A., Venere, M., DiTullio, R.A., Jr., and Halazonetis, T.D. (2003). 53BP1 and NFBD1/MDC1-Nbs1 Function in Parallel Interacting Pathways Activating Ataxia-Telangiectasia Mutated (ATM) in Response to DNA Damage. Cancer Res. *63*, 8586–8591.

Murshudov, G.N., Vagin, A.A., and Dodson, E.J. (1997). Refinement of macromolecular structures by the maximum-likelihood method. Acta Crystallogr. D Biol. Crystallogr. *53*, 240–255.

Otwinowski, Z., and Minor, W. (1997). Processing of X-ray diffraction data collected in oscillation mode. Methods Enzymol. *276*, 307–326.

Paull, T.T., Rogakou, E.P., Yamazaki, V., Kirchgessner, C.U., Gellert, M., and Bonner, W.M. (2000). A critical role for histone H2AX in recruitment of repair factors to nuclear foci after DNA damage. Curr. Biol. *10*, 886–895.

Peng, A., and Chen, P.L. (2003). NFBD1, like 53BP1, is an early and redundant transducer mediating Chk2 phosphorylation in response to DNA damage. J. Biol. Chem. *278*, 8873–8876.

Petersen, S., Casellas, R., Reina-San-Martin, B., Chen, H.T., Difilippantonio, M.J., Wilson, P.C., Hanitsch, L., Celeste, A., Muramatsu, M., Pilch, D.R., et al. (2001). AID is required to initiate Nbs1/gamma-H2AX focus formation and mutations at sites of class switching. Nature *414*, 660–665.

Redon, C., Pilch, D., Rogakou, E., Sedelnikova, O., Newrock, K., and Bonner, W. (2002). Histone H2A variants H2AX and H2AZ. Curr. Opin. Genet. Dev. *12*, 162–169.

Rodriguez, M., Yu, X., Chen, J., and Songyang, Z. (2003). Phosphopeptide binding specificities of BRCA1 COOH-terminal (BRCT) domains. J. Biol. Chem. *278*, 52914–52918.

Rogakou, E.P., Pilch, D.R., Orr, A.H., Ivanova, V.S., and Bonner, W.M. (1998). DNA double-stranded breaks induce histone H2AX phosphorylation on serine 139. J. Biol. Chem. *273*, 5858–5868.

Rogakou, E.P., Boon, C., Redon, C., and Bonner, W.M. (1999). Megabase chromatin domains involved in DNA double-strand breaks in vivo. J. Cell Biol. *146*, 905–916.

Schultz, L.B., Chehab, N.H., Malikzay, A., and Halazonetis, T.D. (2000). p53 binding protein 1 (53BP1) is an early participant in the cellular response to DNA double-strand breaks. J. Cell Biol. *151*, 1381–1390.

Shang, Y.L., Bodero, A.J., and Chen, P.-L. (2003). NFBD1, a novel nuclear protein with signature motifs of FHA and BRCT, and an internal 41-amino acid repeat sequence, is an early participant in DNA damage response. J. Biol. Chem. *278*, 6323–6329.

Shiozaki, E.N., Gu, L., Yan, N., and Shi, Y. (2004). Structure of the BRCT repeats of BRCA1 bound to a BACH1 phosphopeptide: implications for signaling. Mol. Cell *14*, 405–412.

Stewart, G.S., Wang, B., Bignell, C.R., Taylor, A.M.R., and Elledge, S.J. (2003). MDC1 is a mediator of the mammalian DNA damage checkpoint. Nature *421*, 961–966.

Stiff, T., O'Driscoll, M., Rief, N., Iwabuchi, K., Lobrich, M., and Jeggo, P.A. (2004). ATM and DNA-PK function redundantly to phosphorylate H2AX after exposure to ionizing radiation. Cancer Res. *64*, 2390–2396.

Terwilliger, T.C., and Berendzen, J. (1999). Automated MAD and MIR structure solution. Acta Crystallogr. D Biol. Crystallogr. *55*, 849–861.

Veuger, S.J., Curtin, N.J., Smith, G.C., and Durkacz, B.W. (2004). Effects of novel inhibitors of poly(ADP-ribose) polymerase-1 and the DNA-dependent protein kinase on enzyme activities and DNA repair. Oncogene *23*, 7322–7329.

Ward, I.M., Minn, K., Jorda, K.G., and Chen, J. (2003). Accumulation of checkpoint protein 53BP1 at DNA breaks involves its binding to phosphorylated histone H2AX. J. Biol. Chem. *278*, 19579–19582.

Williams, R.S., Green, R., and Glover, J.N. (2001). Crystal structure of the BRCT repeat region from the breast cancer-associated protein BRCA1. Nat. Struct. Biol. *8*, 838–842.

Williams, R.S., Lee, M.S., Hau, D.D., and Glover, J.N. (2004). Structural basis of phosphopeptide recognition by the BRCT domain of BRCA1. Nat. Struct. Mol. Biol. *11*, 519–525.

Wiseman, T., Williston, S., Brandts, J.F., and Lin, L.N. (1989). Rapid measurement of binding constants and heats of binding using a new titration calorimeter. Anal. Biochem. *179*, 131–137.

Xie, A., Puget, N., Shim, I., Odate, S., Jarzyna, I., Bassing, C.H., Alt, F.W., and Scully, R. (2004). Control of sister chromatid recombination by histone H2AX. Mol. Cell *16*, 1017–1025.

Xu, X., and Stern, D.F. (2003). NFBD1/MDC1 regulates ionizing radiation-induced focus formation by DNA checkpoint signaling and repair factors. FASEB J. *17*, 1842–1848.

Yaffe, M.B., and Cantley, L.C. (2000). Mapping specificity determinants for protein-protein association using protein fusions and random peptide libraries. Methods Enzymol. *328*, 157–170.

You, Z., Chahwan, C., Bailis, J., Hunter, T., and Russell, P. (2005). ATM activation and its recruitment to damaged DNA require binding to the C terminus of Nbs1. Mol. Cell. Biol. *25*, 5363–5379.

Yu, X., Chini, C.C., He, M., Mer, G., and Chen, J. (2003). The BRCT domain is a phospho-protein binding domain. Science *302*, 639–642.

## Accession Numbers

Coordinates have been deposited with the Protein Data Bank with the ID code 2AZM.